Published in final edited form as:
Cell. 2014 June 5; 157(6): 1339–1352. doi:10.1016/j.cell.2014.05.012.

Increased Adipocyte O_2 Consumption Triggers HIF-1α Causing Inflammation and Insulin Resistance in Obesity

Yun Sok Lee[1,8], **Jung-whan Kim**[2,8,10], **Olivia Osborne**[1], **Da Young Oh**[1], **Roman Sasik**[1], **Simon Schenk**[3], **Ai Chen**[1], **Heekyung Chung**[1], **Anne Murphy**[4], **Steven M. Watkins**[5], **Oswald Quehenberger**[1], **Randall S. Johnson**[6,7,9], and **Jerrold M. Olefsky**[1,9]

[1]Department of Medicine, Division of Endocrinology and Metabolism, University of California, San Diego, La Jolla, CA 92093, USA

[2]Molecular Biology Section, Division of Biological Sciences, University of California, San Diego, La Jolla, CA 92093, USA

[3]Department of Orthopaedic Surgery, University of California, San Diego, La Jolla, CA 92093, USA

[4]Department of Pharmacology, University of California, San Diego, La Jolla, CA 92093, USA

[5]Lipomics Technologies, Inc., West Sacramento, CA 95691, USA

[6]Department of Cell and Molecular Biology, Karolinska Institute, Stockholm, SE-171 77, Sweden

[7]Department of Physiology, Development and Neuroscience, University of Cambridge, Cambridge, CB2 3EG, United Kingdom

Summary

Adipose tissue hypoxia and inflammation has been causally implicated in obesity-induced insulin resistance. Here we report that early in the course of high fat diet (HFD) feeding and obesity, adipocyte respiration becomes uncoupled, leading to increased oxygen consumption and a state of relative adipocyte hypoxia. These events are sufficient to trigger HIF-1α induction, setting off the chronic adipose tissue inflammatory response characteristic of obesity. At the molecular level, these events involve saturated fatty acid stimulation of the adenine nucleotide translocase 2

[9]Address correspondence to Jerrold M. Olefsky, M.D., Department of Medicine, Division of Endocrinology and Metabolism, University of California, San Diego, La Jolla, CA 92093, USA Tel: 858-534-6651, Fax: 858-534-6653, jolefsky@ucsd.edu and Randall S. Johnson, Ph.D., Department of Physiology, Development and Neuroscience, University of Cambridge, Cambridge, UK CB2 3EG, Telephone +44 1223 765931, rsj33@cam.ac.uk.
[8]These authors contributed equally to this work.
[10]Current Address: Department of Molecular and Cell Biology, University of Texas at Dallas, Richardson, TX 75080, USA

Author Contributions: Y.S.L. designed and performed the majority of the experiments. J.-W.K. designed and performed the majority of the experiments. Y.S.L. and J.-W.K. contributed equally to this work. O.O. and D.Y.O conducted clamp experiments and monocyte tracking experiments. R.S. analyzed ChIP-Seq data. S.S., A.C and A.M. helped to measure muscle insulin sensitivity and mitochondrial activity. H.C. helped to measure RNA and protein expression. S.M.W. and O.Q. conducted lipid analysis. R.S.J and J.M.O conceived and supervised the project.

No potential conflicts of interest relevant to this article were reported.

(ANT2), an inner mitochondrial membrane protein, which leads to the uncoupled respiratory state. Genetic or pharmacologic inhibition of either ANT2 or HIF-1α can prevent or reverse these pathophysiologic events, restoring a state of insulin sensitivity and glucose tolerance. These results reveal the sequential series of events in obesity-induced inflammation and insulin resistance.

Keywords

Obesity; Insulin resistance; Adipose tissue hypoxia; Uncoupled Respiration; Hypoxia inducible factor; Adipose tissue inflammation

Introduction

Obesity is characterized by low-grade chronic inflammation in adipose tissue, liver and skeletal muscle (Glass and Olefsky, 2012; Shu et al., 2012). This inflammatory state progresses during the course of obesity and can lead to systemic insulin resistance, hyperinsulinemia and glucose intolerance (Lee et al., 2011b). In obesity, adipocyte hypertrophy, combined with compromised adipose tissue vascularization restricts oxygen availability leading to areas of adipose tissue hypoxia (Pasarica et al., 2009), and recent evidence suggests that this can cause adipose tissue dysfunction in obesity (Hosogai et al., 2007). The hypoxia response is largely mediated by hypoxia inducible factors (HIFs). HIFs are heterodimeric basic helix-loop-helix transcription factors composed of two dimeric subunits: an oxygen-sensitive α subunit and a ubiquitously and constitutively expressed β subunit, HIF-1β (ARNT) (Keith et al., 2012). There are 2 major α subunits, HIF-1α and HIF-2α, which are differentially regulated by oxygen tension and metabolic signals (Keith et al., 2012). Under normal conditions, α subunits are hydroxylated by prolyl hydroxylases (PHDs), which allows the ubiquitin ligase, Von Hippel-Lindau tumor suppressor (VHL) to ubiquitinate HIF-1α, which is then targeted for proteolytic degradation via the proteasomal pathway. The hydroxylation step is inhibited under hypoxic conditions, leading to stabilization and increased expression of HIF-1α. HIF-1α and HIF-2α regulate different subsets of genes, although they can share common targets such as *VEGF* and *GLUT1* (Keith et al., 2012). In arginine homeostasis, HIF-1α induces *iNOS* expression and increases nitric oxide (NO) production from arginine, whereas HIF-2α stimulates *arginase* expression, and suppresses NO production (Branco-Price et al., 2012; Melillo et al., 1996; Takeda et al., 2010). Therefore, identification of differential roles of adipocyte HIF-1α and HIF-2α is essential to understand the molecular mechanisms of the metabolic consequences of adipose tissue hypoxia in obesity.

Recently, it has been reported that adipocyte-specific HIF-1α overexpressing mice develop insulin resistance with increased adipose tissue inflammation due to induction of the fibrotic program (Halberg et al., 2009). Deletion of either *HIF-1β* or *HIF-1α* in adipocytes protects mice from high-fat diet (HFD)-induced insulin resistance (Jiang et al., 2011; Krishnan et al., 2012; Lee et al., 2011a). Deletion of HIF-1β results in the loss of transcriptional activity of both HIF-α factors, and other factors that bind HIF-1β, such as the Aryl hydrocarbon receptor (AhR) with which HIF-1β also dimerizes. Loss of HIF-1α alone may cause

phenotypic effects chiefly related to the remaining activity of HIF-2α. Thus, the effect of HIF-1α vs HIF-2α needs to be established to understand their roles in adipocyte metabolism and obesity. To assess these issues, we generated *HIF-1α* adipocyte KO (HAKO), *HIF-2α* adipocyte KO (H2AKO), and *HIF-1α* and *HIF-2α* double adipocyte KO (DHAKO) mice, and analyzed their metabolic phenotypes and underlying mechanisms. We found that obesity leads to adenine nucleotide translocase (ANT)-mediated uncoupled respiration, increased adipocyte oxygen consumption and a state of relative hypoxia, triggering induction of HIF-1α. Adipocyte *HIF-1α* deletion results in decreased inflammation and insulin resistance while *HIF-2α* ablation caused increased inflammation and insulin resistance.

Results

Adipocyte Oxygen Consumption Increases on HFD

Recently, it has been shown that oxygen tension decreases in adipose tissue of obese subjects and obese animal models (Halberg et al., 2009; Pasarica et al., 2009). Consistent with this, we observed that adipocyte hypoxia is induced as early as 1 and 3 days of HFD, as measured by staining of hypoxia adducts with pimonidazole (Figures 1A and S1A). Moreover, HIF-1a protein levels, *VEGF* mRNA (a well known HIF-1α target gene) expression and lactate accumulation (a hypoxic respiration product) were also markedly increased by 3 days of HFD (Figures 1B-1D and S1B). Hypoxia is induced by an imbalance between oxygen supply and consumption, and the hypoxia literature shows that increased tissue oxygen consumption (Doege et al., 2005; Hagen et al., 2003; Sato et al., 2011) can be a major cause of relative tissue hypoxia. To test this, we isolated primary adipocytes from lean and HFD/obese mice, and found that oxygen consumption rate was significantly increased by HFD (Figure 1E). This effect was observed in adipocytes isolated from both short-term (3 days) and chronic (30 weeks) HFD-fed mice. Interestingly, this increase was not abrogated by oligomycin treatment, suggesting an increase in uncoupled respiration. Therefore, it seems reasonable to conclude that an important mechanism for relative adipocyte hypoxia with HFD and obesity is related to increased uncoupled utilization of oxygen.

Adipose tissue is exposed to high circulating free fatty acid (FFA) levels in obesity (Figure S1C), and to directly assess adipocyte FFA exposure, we measured total FFA levels within the epididymal adipose fat pads. This lipid fraction is distinct from triacylglycerols and diacylglycerols (Figure S1D), and as Figure 1F shows, adipose tissue FFA levels were elevated at 3, 7 days and 15 weeks of HFD. To test whether FFAs can increase oxygen consumption, we incubated 3T3-L1 adipocytes with different FFAs such as myristrate, laurate, and palmitate. As seen in Figure 1G, the oxygen consumption rate was significantly increased by the different saturated FAs (SFAs). Interestingly, oxygen consumption was not increased by the TLR4-specific ligand Kdo2-Lipid A (KLA) (Sims et al., 2010), showing that the FFA-mediated increase in adipocyte oxygen consumption was not due to TLR4 activation (Figure 1G).

SFAs Increase O_2 Consumption by Stimulating ANT2

ANT1 and 2 are mitochondrial inner membrane proteins which pump protons out of the intermembrane space into the mitochondrial matrix (Andreyev et al., 1988). Thus, excessive ANT activity will cause proton leakage from the intermembrane space, leading to uncoupled respiration (Brand et al., 2005). In theory, SFAs can increase oxygen consumption by increasing FA oxidation or by activating the ANT-dependent uncoupling of oxidative metabolism. To assess these possibilities, we treated adipocytes with palmitate in the presence or absence of inhibitors of carnitine palmitoyl transferase-1 or ANT. As seen in Figure 1G, the FFA-dependent increase in oxygen consumption was suppressed by the ANT inhibitor, carboxyatractyloside (CAtr), whereas, inhibition of carnitine-palmitoyl transferase with etomoxir or treatment with oligomycin did not attenuate the FFA effect (Figure 1H). Consistent with this, ATP production was not increased by palmitate treatment (Figure 1I), further showing that the FFA-induced increase in oxygen consumption was due to ANT-mediated uncoupling of oxidative metabolism rather than increased FA oxidation.

Incubation of 3T3-L1 adipocytes with palmitate increased HIF-1α protein expression and mRNA levels of HIF-1α target genes, as well as the number of cells staining positive for pimonidazole adducts (Figures 1J, 1K and S1E). Both of these effects were blunted by co-treatment with CAtr (Figure 1K). Furthermore, acute in vivo treatment of mice with CAtr reduced the number of hypoxic adipocytes in epididymal white adipose tissue (eWAT) in 3 day HFD mice (Figure 1L). These results support the view that HFD causes an increase in adipocyte oxygen consumption due to ANT-mediated uncoupled respiratory metabolism (Figure 1E), leading to a state of relative adipocyte hypoxia and induction of the HIF-1α transcriptional program.

ANT Inhibition Ameliorates Adipose Tissue Hypoxia, Inflammation and Insulin Resistance in HFD/Obese Mice

In mice, 3 isoforms of ANT have been identified: ANT1, ANT2 and ANT4 (Zhivotovsky et al., 2009). As seen in Figure 2A, ANT1, ANT2 and UCP2 are abundantly expressed in white adipocytes, whereas expression of ANT4, UCP1 and UCP3 is negligible. HFD slightly decreased ANT1 expression (Figure 2A), while ANT2 was was reduced by ∼ 25% at 15 weeks of HFD (Figure 2A). UCP2 was decreased by 43% by HFD (Figure 2A). These results suggest that, unlike brown adipocytes, which are more UCP1/3-dependent (Figure S2), uncoupled respiration in HFD white adipocytes is largely mediated by ANTs.

To determine the relative contribution of ANT1 and ANT2 to SFA-induced adipocyte uncoupled respiration, we used RNAi to knockdown (KD) ANT1, or ANT2, or both, in 3T3-L1 adipocytes. These studies revealed a reciprocal relationship between ANT1 and ANT2, such that when ANT1 was depleted, ANT2 expression increased while KD of ANT2 caused an increase in ANT1. This was fortuitous, allowing us to dissect the roles of these 2 isoforms in basal vs FA-stimulated respiration. When ANT1 was depleted, the basal respiration rate was substantially diminished, but the effect of palmitate was still present, although moderate (Figure 2B). With ANT2 KD, basal respiration went up (because ANT1 was increased with the ANT2 knockdown), whereas, the effect of palmitate to stimulate respiratory rates was completely ablated (Figure 2B). KD of both ANT1 and ANT2

decreased the basal respiration rate and abrogated the effect of palmitate. These data indicate that ANT1 is mostly responsible for the basal rate of mitochondrial respiration and that ANT2 is the major target of fatty acid stimulation. To extend this KD approach to the in vivo situation, we generated an adenovirus-associated viral (AAV) vector expressing anti-ANT2 shRNA, and injected this or a control anti-luciferase shRNA AAV vector into epididymal fat pads of WT mice. Three weeks after injection, the mice were placed on HFD. After 3 days of HFD, ANT2 was depleted by ∼80% and pimonidazole adduct staining was decreased by ∼60% (Figure 2C). Collectively, these data indicate that activation of ANT2 causes the palmitate-induced increase in uncoupled respiration and the state of relative adipocyte hypoxia.

To test whether inhibition of ANT activity and adipocyte hypoxia can protect HFD/obese mice from adipose tissue inflammation and glucose intolerance, we treated 10 week HFD mice with lower doses of CAtr (0.4 and 1.0 mg/kg) for 9 days. As seen in Figure 2D, 0.4 mg/kg and 1.0 mg/kg of CAtr reduced the number of hypoxic adipocytes and adipose tissue macrophages (ATMs) without change in body weight or blood oxygen saturation (Figures 2E and 2F). Interestingly, adipose tissue mass was significantly increased by CAtr treatment (Figure 2G). CAtr treatment improved glucose and insulin tolerance and reduced hyperinsulinemia in HFD mice (Figures 2H and 2I), indicating that chronic inhibition of the ANT-dependent increase in uncoupled adipocyte respiration ameliorates adipocyte hypoxia, adipose tissue inflammation, glucose intolerance and insulin resistance in chronic HFD/obese mice.

Adipocyte HIF-1α KO Facilitates Fat Mobilization from Liver to Adipose Tissue

We next studied the effect of adipocyte *HIF-1α* deletion by generating *HIF-1α* adipocyte KO (HAKO) mice (Figures S3A and S3B). *HIF-1α* deletion was restricted to adipocytes, with no deletion detected in stromal vascular cells (SVCs), muscle, liver, or intraperitoneal (IP) macrophages (Figure S3A). As expected, *HIF-1α* was quantitatively deleted in interscapular brown adipose tissue (BAT) (Figure S3A) as well as WAT. UCP1-3 expression in BAT was the same in WT vs HAKO mice (Figure S2). The HAKO mice exhibited normal body weight on either chow or HFD with no differences in food intake compared to WT controls (Figure S3C). In obesity, hypoxia can induce adipose tissue fibrosis, restricting adipocyte expansion and lipid storage (Halberg et al., 2009). In HAKO mice, adipose tissue fibrosis was markedly reduced on HFD as measured by trichrome staining (Figure S3D) with a concomitant increase in adipose tissue mass and mean adipocyte size (Figures S3E to S3H). Oxygen consumption rate in HAKO eWAT adipocytes was comparable to WT adipocytes on normal chow diet (NCD), but was higher on HFD (Figure S3I), consistent with the view that one function of the HIF-1α response is to decrease oxygen consumption in an attempt to mitigate hypoxia. Adipose tissue vascular density as measured by CD31 positive staining of eWAT was not changed in HAKO mice (Figure S3J). Hepatic TG content was significantly decreased in HAKO mice (Figures S3K and S3L), indicating a redistribution of lipid stores from liver to adipocytes on HFD. Interestingly, expression of inflammatory genes such as TNFα and IL-1β, as well as the lipogenic gene fatty acid synthase, were decreased in the liver of HAKO mice (Figure S3M).

Adipocyte HIF-1α KO Protects from HFD-Induced Insulin Resistance

Glucose tolerance was comparable between WT and HAKO mice on NCD, whereas, the KO mice exhibited improved glucose tolerance with reduced plasma insulin levels on HFD (Figures 3A to 3C). These findings suggested protection from HFD-induced insulin resistance and this concept was confirmed with insulin tolerance tests (ITTs), which showed a greater glucose lowering effect of insulin in the HAKO compared to WT mice (Figure 3D). To quantitate overall insulin sensitivity and to determine tissue-specific contributions, hyperinsulinemic-euglycemic clamp studies were performed. As seen in Figure 3E, the glucose infusion rate (GIR) required to maintain euglycemia was substantially higher in HFD-fed HAKO mice compared to WT. Furthermore, insulin-stimulated glucose disposal rate (IS-GDR), insulin suppression of hepatic glucose production (HGP) and suppression of circulating FFA levels were all markedly increased in HAKO mice, demonstrating that adipocyte HIF-1αdeletion leads to systemic insulin sensitivity in muscle, liver, and adipose tissue on HFD. Consistent with these results, ex vivo studies in primary isolated adipocytes demonstrated improved stimulation of glucose transport in KO compared with WT adipocytes from HFD mice (Figure 3F).

Adipocyte HIF-1α KO Protects from HFD-Induced Adipose Tissue Inflammation

To test the potential role of HIF-1α in adipose tissue inflammation in the context of obesity, we analyzed ATMs in WT and HAKO mice on NCD or HFD. Immunohistochemistry revealed decreased ATMs in HAKO mice on HFD compared to WT (Figure 4A). Next, we performed flow cytometry studies on stromal vascular cells (SVCs) from WT and HAKO adipose tissue on a NCD or HFD. As seen in Figure 4B, the ratio of CD11b and F4/80 double positive ATMs or M1-like polarized CD11b, F4/80, and CD11c triple positive ATMs was markedly decreased in adipose tissue from HFD HAKO mice. Consistent with these results, mRNA expression of macrophage marker genes such as *F4/80* and *CD11b*, and inflammatory genes such as *TNFα, IL-6, Rantes, MIP-1α, MCP-1*, and *CYR61* was reduced in HAKO adipose tissue (Figure 4C). Moreover, expression of major histocompatibility complex (MHC) class II genes such as *H2-Aa*; and *CD74*, which are increased in obese human adipocytes (Deng et al., 2013), were also reduced in primary adipocytes of HAKO mice (Figure 4D). Lastly, plasma levels of MCP-1 and resistin were reduced, whereas, circulating adiponectin was increased in HAKO mice (Figure 4E).

In macrophages and endothelial cells, HIF-1α can lead to the induction of chemoattractive factors such as MCP-1 and Leukotriene B4 (LTB4) (Gonsalves and Kalra, 2010; Spite et al., 2011). Thus, we measured adipocyte-conditioned media (ACM)-induced chemotaxis in Transwell dishes. As seen in Figure 4F, migration of Raw264.7 macrophages to HAKO ACM was decreased compared with WT ACM. Moreover, mRNA level of *5-lipoxygenase-activating protein* (*FLAP)*, the enzyme producing LTB4, and production of LTB4 from primary HAKO adipocytes was decreased in HAKO adipose tissue (Figures 4G and 4H). To directly assess the mechanistic links between hypoxia, HIF-1α and chemokine release, we conducted in vitro studies in 3T3-L1 adipocytes. These experiments showed that under hypoxic conditions, expression of a wide array of proinflammatory adipocyte genes was increased, including *FLAP* and *MCP-1* (Figures S4A and S4B), while the hypoxia-dependent increase in *MCP-1, FLAP, and iNOS* expression was reduced by HIF-1α

knockdown (Figure S4B). Chromatin immunoprecipitation sequence analysis revealed that HIF-1α binds to the *FLAP* and *p65* (NF-κB) gene promoters under hypoxic conditions (Figure S4C). A heat map also shows occupancy of other inflammatory pathway genes and hypoxia target genes by HIF-1α. Furthermore, ACM harvested from hypoxic 3T3-L1 adipocytes elicited greater macrophage chemotaxis than normoxic ACM, and the hypoxia-dependent increase was reduced in HIF-1α knockdown adipocytes (Figure S4D).

To assess chemotaxis in vivo, we conducted macrophage tracking studies. With this approach, WT blood monocytes were obtained from a donor mouse and labeled ex vivo with fluorescent PKH26 dye. The fluorescently labeled monocytes were then injected into HFD WT or HAKO recipient mice and the appearance of the labeled cells as ATMs was measured. As seen in Figure 4I, a marked decrease in labeled ATM appearance was observed in the HAKO mice compared with WT. FACS analysis showed that this was due to a decrease in the proinflammatory F4/80, CD11b, CD11c triple positive ATM population (Figure 4I, 3rd set of bars), with an increase in the non-inflammatory CD11c(-) ATMs (righthand bars). Taken together, these results indicate that HIF-1α can play a key initiating role in adipose tissue ATM accumulation and inflammation by stimulating chemokine and LTB4 production in obesity.

HIF-1α Increases Production of NO and Lactate in Adipocytes

Previously, it was shown that HIF-1α stimulates NO production by inducing *iNOS* expression in macrophages (Takeda et al., 2010). Interestingly, NO can attenuate insulin signaling through nitrosylation of insulin signaling molecules, such as Akt, and this suppresses Akt phosphorylation/activation (Yasukawa et al., 2005). Thus, we measured mRNA levels of *iNOS* and *arginase 1* in primary adipocytes and SVCs in eWAT from WT or HAKO mice. As shown in Figure 5A, *iNOS* expression was induced in adipocytes and SVCs by HFD, and this effect was blunted in cells from HAKO mice. HFD also led to increased *arginase 1* expression, and this increase was enhanced in HAKO mice. Thus, the *iNOS/arginase* ratio was markedly reduced in HAKO adipose tissue. As would be predicted from these gene expression changes, levels of adipose tissue NO_2, a stable breakdown product of NO, were induced ∼3 fold on HFD in WT mice, and this increase was almost completely abrogated in HAKO mice (Figure 5B). Consistent with these changes in NO levels, nitrosylation of total protein, including Akt, was increased on HFD and was reduced in HAKO adipose tissue (Figure 5C). Concomitant with this, insulin-stimulated Akt phosphorylation was greater in adipose tissue from HFD HAKO versus WT mice (Figure 5D).

Since adipose tissue is one of the major sources of lactate production (DiGirolamo et al., 1992; Qvisth et al., 2007), we hypothesized that HIF-1α increases lactate production from hypoxic HFD adipocytes, contributing to increased basal hepatic glucose production and higher fasting blood glucose levels. In HFD WT adipose tissue, expression *of PDK1, 2*, and *4* were increased, and these changes were blunted in adipose tissue from HFD HAKO mice (Figure 5E). Consistent with this, HAKO mice exhibited lower basal HGP rates and lactate content in adipose tissue on HFD (Figures 5F and 5G) with reduced basal blood glucose levels (Figure 3B). These data suggest that adipocyte hypoxia and HIF-1α activation

stimulate lactate production from adipocytes, which supports increased hepatic glucose production and elevated basal blood glucose levels.

*HIF-2α*KO Exacerbates HFD-Induced Inflammation and Insulin Resistance

Recently, opposing roles of HIF-1α and HIF-2α have been suggested in macrophages and in cancer progression (Keith et al., 2012). In adipose tissue, HFD decreases HIF-2α protein levels, whereas, it induces HIF-1α expression (Jiang et al., 2011). To examine the role of HIF-2α in adipose tissue, we generated adipocyte-specific *HIF-2α* (H2AKO) and double HAKO/H2AKO mice (DHAKO) (Figures 6A and S5A). H2AKO mice exhibited normal body weight on NCD, but were slightly heavier on HFD without changes in eWAT mass (Figures 6B and 6C). While glucose tolerance was normal on NCD in H2AKO (Figure 6D), on HFD, H2AKO mice exhibited more severe glucose intolerance and hyperinsulinemia compared with WT (Figures 6E and 6F), indicating a greater susceptibility to HFD-induced insulin resistance. Confirming this formulation, ITTs showed an impaired glucose lowering effect of insulin in H2AKO mice (Figure 6G). Next, we measured adipose tissue inflammation using flow cytometry analyses of SVCs. As seen in Figure 6H, the percentage of CD11b and F4/80 double positive, or M1-like CD11b, F4/80, and CD11c triple positive ATMs was increased in H2AKO HFD adipose tissue. mRNA expression of inflammatory genes such as *FLAP*, *IL-6* and *TNFα* was also increased in HFD H2AKO adipocytes and adipose tissue (Figures 6I and S5B). Expression of fibrosis-related genes such as *Col-1a*, *Col-3a*, and *lysyl oxidase* was reduced (Figure S5C), suggesting that impaired glucose tolerance in H2AKO mice was not associated with adipose tissue fibrosis. Taken together, these results show that HIF-2α can attenuate HFD-induced inflammation, glucose intolerance and insulin resistance.

The HAKO Phenotype Dominates in Double *HIF-1α* and *-2α* KO Mice

Since HIF-1α and HIF-2α can be interactive, we studied double DHAKO mice (Figure 7A). DHAKO mice exhibited normal body weight on HFD (Figure 7B). These mice displayed increased eWAT mass and adipocyte size with reduced adipose tissue fibrosis upon HFD (Figures 7C and 7D). Glucose tolerance was normal on NCD, whereas, on HFD, glucose and insulin tolerance were significantly improved with lower insulin levels (Figures 7E to 7H). Hyperinsulinemic euglycemic clamp studies revealed increased GIR, IS-GDR, greater suppression of HGP and FFA levels in the DHAKO mice, indicating improved systemic insulin sensitivity in muscle, liver, and adipose tissue (Figure 7I). Along with these metabolic changes, the HFD-dependent increase in ATM accumulation and M1-like polarization was significantly reduced in the DHAKO mice (Figure 7J). Nitrite accumulation in adipose tissue was also decreased in the DHAKO mice (Figure 7K). Thus, while adipocyte *HIF-2α* deletion leads to greater inflammation, glucose intolerance and insulin resistance, the double KOs completely phenocopy the results with the HAKO mice. This indicates that loss of both isoforms mirrors the results seen with loss of *HIF-1α*, indicating that the main effect of HIF-2α is to counteract HIF-1α.

Discussion

It is now well-established that adipose tissue inflammation is an important component of the obese state, and that this inflammatory response is a major contributor to the systemic insulin resistance which characterizes obesity and type 2 diabetes (Glass and Olefsky, 2012). However, the early events that initiate this inflammatory response are less well understood and are obviously central to defining the etiology of the insulin resistant, inflammatory state. Our data demonstrate that *HIF-1α* mRNA and protein levels are highly induced early in the course of HFD-induced obesity, well before significant adiposity develops. Obviously, HIF-1α induction occurs when cells sense hypoxia, and our data show that SFA stimulation of ANT2 causes increased adipocyte oxygen consumption due to uncoupled mitochondrial respiration, leading to a state of relative cellular hypoxia; this triggers HIF-1α expression, and induces adipocyte chemokine production with increased ATM content and tissue inflammation. This results in glucose intolerance and insulin resistance (Figure S5D), all of which are mitigated by adipocyte *HIF-1α* deletion or ANT2 inhibition. With this scenario, adipocyte hypoxia and induction of HIF-1α function as early triggers for inflammation and insulin resistance.

It is commonly assumed that in obese adipose tissue, enlarging adipocytes outstrip the perfused blood oxygen supply, resulting in areas of microhypoxia. While decreased adipose tissue oxygen tension exists in obese adipose tissue (Pasarica et al., 2009), the hypoxia literature suggests that in non-ischemic tissue, increased cellular oxygen consumption is often the major, or at least an important, contributing factor to relative cellular hypoxia (Hagen et al., 2003). Indeed, our current studies demonstrated that oxygen consumption is markedly elevated in eWAT adipocytes obtained from HFD/obese mice compared to lean mice. This leads to a state of relative adipocyte hypoxia with HIF-1α induction and proinflamamtory signalling. All of these effects were seen after as early as 1 and 3 days of HFD.

Furthermore, our results indicate that the mechanism for this uncoupled respiration relates to the elevated FFA levels commonly seen in obesity. In the context of HFD and obesity, there are several ways in which increased fatty acid availability could occur. First, increased adipocyte lipolysis, particularly in visceral fat, is a well-known early characteristic of the obese state (Nielsen et al., 2004), and, as a later event, adipocyte insulin resistance leads to decreased anti-lipolytic effects of insulin which would further increase these local fatty acid levels. The intracellular concentration of FFAs is likely to be even higher in adipocytes, since up to 50% of FAs hydrolyzed from the TG droplet can be directed towards re-esterification (Leibel et al., 1985). Finally, HFD leads to an increased systemic fat load due to incoming chylomicrons which are subsequently hydrolyzed at tissue sites, giving rise to increased tissue fatty acid exposure. While the proportional contribution of each of these components to overall FA exposure needs to be determined, our data directly show a 2-4 fold elevation in adipose tissue FFA levels as early as 3 days on HFD. We found strong evidence that SFAs can cause uncoupled adipocyte respiration by demonstrating that SFA treatment of 3T3-L1 adipocytes directly leads to increased oxygen consumption by activation of ANT2. This mechanism translated to the in vivo situation, since depletion of epididymal adipose tissue ANT2 led to decreased adipose hypoxia in HFD mice. In addition,

treatment of obese mice with the ANT inhibitor, CAtr, greatly reduced the number of hypoxic adipocytes. In vivo CAtr administration also led to decreased adipose tissue inflammation, and, most importantly, improved glucose tolerance with increased insulin sensitivity. Taken together, our results support the idea that SFAs increase oxygen consumption by facilitating ANT2-mediated uncoupled respiration and that this is a key contributor to relative cellular hypoxia in obesity triggering the HIF-1α response. This is likely to be a major mechanism for adipose tissue hypoxia, since one would not expect decreased oxygen perfusion after 1 day of HFD, when adipose tissue expansion and remodeling have not yet occurred.

In our KO mouse studies, genetic deletion of HIF-1α from adipocytes is sufficient to cause systemic insulin sensitivity in liver and muscle. This emphasizes the degree to which adipose tissue can communicate to other key insulin target tissues, and indicates the primacy of changes in adipose tissue in the context of systemic insulin action. It is also important to note that with adipocyte HIF-1α deletion, not only did inflammation decrease in adipose tissue, but it also was markedly reduced in liver. This indicates another potential way in which adipose tissue can signal to other tissues, since it is likely that the decreased hepatic inflammation is secondary to the primary changes in adipose tissue.

We found that the ratio of *iNOS* to *arginase* was increased in HFD adipose tissue and primary adipocytes, leading to increased generation of NO. Previous reports have shown that NO can result in decreased cellular insulin sensitivity by causing inhibitory nitrosylation of Akt (Yasukawa et al., 2005) and that *iNOS* KO mice are protected from HFD-induced insulin resistance (Perreault and Marette, 2001). Consistent with this, we found that nitrosylation of Akt is increased in HFD adipose tissue and that this is associated with decreased insulin stimulated Akt phosphorylation. We also show a decreased adipose tissue *iNOS/arginase* ratio in the HAKO mice, resulting in less NO production with decreased Akt nitrosylation and improved insulin-stimulated Akt phosphorylation. This suggests that inflammation-mediated increased tissue NO production, with Akt nitrosylation, is a cytokine-independent mechanism for obesity-induced insulin resistance and that attenuation of this NO effect is a component of the enhanced insulin sensitivity observed in the HAKO mice.

In contrast to the beneficial effects *of HIF-1α* KO, deletion of adipocyte *HIF-2α* led to increased inflammation and exacerbation of insulin resistance on HFD. This suggests that HIF-2α normally plays a protective role from obesity-induced decreased insulin sensitivity. Interestingly, in the DHAKO mice, the *HIF-1α* deletion was dominant, since the phenotype of DHAKO and HAKO mice was comparable. One possible explanation for these results is that HIF-1α actively promotes inflammation and impairs insulin sensitivity on HFD, whereas, the protective effects of HIF-2α are accomplished by counteracting HIF-1α.

Previous reports on *HIF-1α* KO or transgenic mice are consistent with our results with respect to the overall metabolic phenotype. For example, ARNT is the heterodimeric binding partner for both HIF-1α and HIF-2α and Jiang et al. and Lee et al. reported that adipocyte-specific deletion of *ARNT* led to protection from HFD-induced obesity, glucose intolerance, and insulin resistance (Jiang et al., 2011; Lee et al., 2011a). In the paper by

Jiang et al., this was accompanied by decreased adipose tissue inflammation. These studies also show protection from HFD-induced weight gain, which was not a feature of our HAKO mice. This is probably due to the fact that *ARNT* deletion has broader effects beyond HIF-1a inhibition, since it would also lead to decreased HIF-2α activity, as well as decreased activity of another ARNT binding partner AhR. On the other hand, Zhang et al. found that transgenic expression of a dominant negative HIF-1α construct in adipose tissue led to obesity and decreased energy expenditure in mice, leaving the relationship between HIF-1α, energy expenditure and weight gain unresolved (Zhang et al., 2010). Finally, Sun et al. show that treatment of mice with a small molecule HIF-1α inhibitor, as well as adipocyte transgenic expression of a dominant negative HIF-1α, led to protection from HFD-induced glucose intolerance, insulin resistance, adipose tissue inflammation and obesity (Sun et al., 2013). In the current studies (Figures S3A and S5A), as well as in past publications (Barak et al., 2002; He et al., 2003; Li et al., 2011), we have shown that aP2-cre expression is highly specific for adipocytes in our aP2 mouse model. Thus, we have found no cre-mediated target gene recombination in muscle, liver, SVCs, or IP macrophages (Figures S3A and S5A). While the majority of studies from other laboratories agree with this (Ahmadian et al., 2011; Chalkiadaki and Guarente, 2012; Polak et al., 2008; Rohm et al., 2013; Sabio et al., 2008), there are a couple of reports showing variable degrees of target gene recombination in macrophages with these aP2 mice (Garcia-Arcos et al., 2013; Paschos et al., 2012). Although our current data in the HAKO and H2AKO mice clearly reveal no evidence for HIF-1α or -2α deletion in macrophages, it is always possible that some degree of recombination might have gone undetected. While some of the detailed findings differ among the various studies, when taken together with the current results, it is clear that *HIF-1α* deletion from adipocytes has beneficial metabolic effects to mitigate HFD-induced adipose tissue inflammation, glucose intolerance and insulin resistance.

The current studies reveal an important role for HIF-1α as an early event that can trigger the adipose tissue inflammatory response, leading to systemic insulin resistance. At the onset of HFD, we find that increased adipocyte oxygen consumption due to uncoupled oxidative metabolism is a major contributor to a state of relative adipocyte hypoxia, providing the stimulus for adipocyte HIF-1α induction. In turn, we have traced the mechanism of uncoupled respiration to the effects of SFAs to stimulate ANT2 activity, which is known to disrupt the mitochondrial membrane proton gradient leading to uncoupled respiration. This leads to the sequential hypothesis (Figure S5D) that elevated FFA levels in obesity provide an early activating event leading to ANT stimulation, uncoupled respiration, with increased oxygen consumption inducing a state relative adipocyte hypoxia. This then triggers the HIF-1α response. In the chronic long term obese setting, the hypoxia is likely exaggerated by an additional component of decreased oxygen perfusion. In turn, HIF-1α stimulates production of the key adipocyte-derived chemokines MCP-1 and LTB4, which drive accumulation of pro-inflammatory ATMs. This leads to a state of adipose tissue inflammation with the subsequent deleterious effects on systemic insulin sensitivity. Once proinflammatory macrophages appear in adipose tissue, they release their own chemokines, setting off a second wave of chemotaxis and ATM accumulation. This then exacerbates the inflammatory/insulin resistance state. In this sequential hypothesis, fatty acid stimulation of ANTs would be an initiating event. The current studies identify early events in the

inflammation/insulin resistance syndrome which provide an improved understanding of these pathophysiologic processes and could lead to new opportunities for therapeutic intervention.

Experimental Procedures

Animals and treatments

To induce adipocyte-specific genetic ablation, mice with homozygous loxP recombinase recognition site-flanked *HIF-1α* or/and *HIF-2α* alleles were bred to mice expressing Cre recombinase driven by *aP2* promoter (Li et al., 2011). Mice were housed in colony cages in 12 h light/12 h dark cycles. For HFD study, mice were subjected to 60% HFD for the indicated time periods (Research Diets, Inc; USA). OGTTs and ITTs were performed as described previously (Lee et al., 2013). Mouse clamp experiments were performed as described previously (Lee et al., 2011b). During the clamps, insulin was infused at a constant rate of 8.0 mU/kg/min. All animal procedures were in accordance with the research guidelines for the use of laboratory animals of University of California, San Diego. Detailed protocols are described in the Extended Experimental Procedures.

Measurement of oxygen consumption

Relative oxygen consumption rate of adipocytes was measured polarographically using Clarke type electrode (Oxytherm, Hansatech Inc.). For oxygen measurements, primary adipocyte were prepared from epididymal adipose tissues from chow or HFD mice with collagenase digestion, or fully differentiated 3T3-L1 adipocytes were detached from plates. Cells were washed with PBS three times and resuspended into HEPES-buffered serum-free DMEM and incubated in the Clarke type electrode chamber maintained at 37°C and continuously stirred. After measurement of oxygen consumption rate, each of the cell suspension was save for total lysate preparation to assess total protein content. Oxygen consumption rate was calculated by normalizing oxygen consumption rate (nmole/sec) to total protein content (μ gs). The effect of FFAs on increasing oxygen consumption in 3T3-L1 adipocytes was confirmed by oxygen measurements using Seahorse XF^{e}96 Analyzer (Seahorse Bioscience).

ANT Knockdown

To knockdown ANT1 or ANT2 in 3T3-L1 adipocytes, duplex siRNAs against mouse ANT1 or ANT2 purchased from Integrated DNA Technology were introduced into 5 day differentiated 3T3-L1 adipocytes using electroporation. For in vivo knockdown of ANT2 in adipose tissue, mice were anesthetized and subjected to laparotomy, and were given 5 injections of 2 ul (2×10^{13} gc/ml) of AAV solution into each epididymal fat pad using a Hamilton syringe. Detailed protocols are described in the Extended Experimental Procedures.

Glucose uptake assays

Glucose uptake in primary adipocytes was measured as described previously (Lee et al., 2008).

Flow cytometry

Flow cytometry analysis of adipose tissue macrophages was performed as described previously (Lee et al., 2011b).

Nitrate and protein nitrosylation measurement

Nitrate content in epididymal adipose tissue lysate was measured using Griess Reagent System (Promega) in accordance with the manufacturer's protocol. Detailed protocols for protein nitrosylation measurement are described in the Extended Experimental Procedures.

Lactate measurement

Lactate content in total adipose tissue lysate was measured by colorimetric lactate assay kit (Biovision, USA).

Macrophage migration assays

In vitro migration of macrophages was measured as described previously (Lee et al., 2011b). For preparation of ACM, primary adipocytes from HFD WT or HFD HAKO were incubated in Dulbecco's Modified Eagle's media supplemented with 0.2% BSA for 12 h. In vivo macrophage tracking experiments was performed as described previously (Oh et al., 2012). Detailed protocols are described in the Extended Experimental Procedures.

Histology

Immunohistochemistry analyses were performed as described previously (Lee et al., 2010; Lee et al., 2011b). For hypoxia staining, NCD or HFD mice were i.p. injected with pimonidazole hydrochloride (60 mg/kg) and/or CAtr (2 mg/kg) 1 h before sacrifice. The mice were anesthetized by an intramuscular injection of a combination of anesthetics, and their adipose tissues were whole-mounted after fixation by vascular perfusion of 1% paraformaldehyde in PBS. Adipose tissue was stained with FITC-conjugated antibodies against pimonidazol adducts (HPI, Inc), which form in hypoxic tissue, and visualized using confocal fluorescence microscopy. For measurement of macrophage or collagen fiber accumulation in adipose tissue, paraffin-embedded tissue sections were stained with anti-F4/80 antibody (Serotech; Cat# MCA497B) or trichrome, respectively. Microscopic images were analyzed using ImageJ software.

Adipose tissue FFA measurement

FFA concentration in adipose tissue was measured by Lipomics, Inc. (West Sacramento, CA). Detailed protocols are described in the Extended Experimental Procedures.

Statistics

The results are shown as means ± SEM. All statistical analyses were performed by Student's *t* test; $P < 0.05$ was considered significant.

Extended Experimental Procedures

Animals and treatments

To induce adipocyte-specific genetic ablation, mice with homozygous loxP recombinase recognition site-flanked *HIF-1α* or/and *HIF-2α* alleles were bred to mice expressing Cre recombinase driven by aP2 promoter (Li et al., 2011). Mice were housed in colony cages in 12 h light/12 h dark cycles. For HFD study, mice were subjected to 60% HFD for the indicated time periods (Research Diets, Inc; USA). For oral glucose tolerance test, the mice were fasted for 6 h and basal blood samples were taken, followed by oral glucose gavage (2 g/kg). Blood samples were drawn at 10, 20, 30, 45, 60, 90 and 120 min after gavage. For ITT, mice were fasted for 6 h, and basal blood samples were taken, followed by intraperitoneal injection of insulin (0.6 U/kg). Mouse clamp experiments were performed as described previously (Lee et al., 2011b). During the clamps, insulin was infused at a constant rate of 8.0 mU/kg/min. All animal procedures were in accordance with the research guidelines for the use of laboratory animals of University of California, San Diego.

Adipose tissue FFA measurement

FFA concentration in adipose tissue was measured by Lipomics, Inc. (West Sacramento, CA). The lipids were extracted from plasma and tissues in the presence of authentic internal standards using chloroform mixed with methanol (2:1 vol/vol) (Folch et al., 1957) and individual lipid classes were separated by HPLC (Cao et al., 2008). Lipid class fractions were transesterified in 1% sulfuric acid (in methanol) in a sealed vial with nitrogen at 100°C for 45 min. Fatty acid methyl esters were extracted from the mixture with hexane containing 0.05% butylated hydroxytoluene, and readied for gas chromatography under nitrogen. Finally, fatty acid methyl esters were separated and quantified by capillary gas chromatography equipped with a 30 m DB-88MS capillary column and a flame-ionization detector.

In vitro pimonidazole adduct formation assay

Differentiated 3T3-L1 adipocytes were pre-incubated in 8% oxygen chamber, similar to in vivo oxygen level in adipose tissue, for 24h for equilibration. Pimonidazole was added to the adipocytes and incubated with or without 100 μM palmitate in the same condition for further 6 h, which was followed by immunocytochemistry analysis of pimonidazole adduct formation.

ANT Knockdown

To knockdown of ANT1 or ANT2 in 3T3-L1 adipocytes, duplex siRNAs against mouse ANT1 or ANT2 purchased from Integrated DNA Technology were introduced into 5 day differentiated 3T3-L1 adipocytes using electroporation. After 2 days of recovery, the cells were detached from the plate and subjected to oxygen consumption measurement or RNA isolation. For in vivo knockdown of ANT2 in adipose tissue, we used an AAV vector system. DNA oligomers for ANT2 shRNA were synthesized according to the “stem-loop” sequences (Valuegene), annealed and cloned into an AAV plasmid. The duplex DNA oligomer was placed downstream of a U6 promoter and the insertion was confirmed by

sequencing. A control vector expressing shRNA against firefly *luciferase* was also constructed. The insert DNA sequence is as follows: ANT2-shRNA-sense, 5′-GATCCGGGCAGATAAGCAATACAAGGTTCAAGAGACCTTGTATTGCTTATCTGCTTTTTC-3′; ANT2-shRNA-antisense, 5′-AATTGAAAAAGCAGATAAGCAATACAAGGTCTCTTGAACCTTGTATTGCTTATCTGCCCG-3′. C57BL/6 mice were injected with AAVs encoding shRNAs against *luciferase* (Lu) or ANT2 into epididymal adipose tissue. 3 weeks later, the mice were switched to HFD or remained on NCD for 3 days, and sacrificed for histology analysis of epididymal adipose tissue. For administration of AAV8-ANT2 shRNA vector to epididymal adipose tissue, mice were anesthetized with ketamine (25 mg/kg), acepromazine (2mg/kg) and xylazine (10 mg/kg), and laparotomy was performed. To distribute the vector in the whole depot, each epididymal fat pad was given 5 injections of 2 ul ($2x10^{13}$ gc/ml) of AAV solution using a Hamilton syringe.

Flow cytometry

Flow cytometry analysis of adipose tissue macrophages was performed as described previously (Lee et al., 2011b). Epididymal adipose tissue were weighed, rinsed three times in PBS, and then minced in FACS buffer (PBS supplemented with 1% low endotoxin BSA). Tissue suspensions were centrifuged at 500g for 5 min and then collagenase-treated (1 mg/mL; Sigma-Aldrich) for 30 min at 37°C with shaking. Cell suspensions were filtered through a 100 μm mesh and centrifuged at 500g for 5 min. SVC pellets were then incubated with erythrocyte lysis buffer (ebioscience) for 5 min before centrifuge (300g; 5 min) and resuspended in FACS buffer. SVCs were incubated with Fc block for 20 min at 4°C before staining with fluorescence labeled primary antibodies or control IgGs for 30 min at 4°C. F4/80-APC FACS antibody was purchased from AbD Serotec (Raleigh, NC); CD11b-fluorescein isothiocyanate and CD11c-PE FACS antibodies were from BD Biosciences. Cells were gently washed twice and resuspended in FACS buffer with propidium iodide (PI) (Sigma-Aldrich). SVCs were analyzed using a FACS Aria flow cytometer (BD Biosciences). Unstained, single stains and Fluorescence Minus One controls were used for setting compensation and gates. The events are first gated based on forward versus side scatter area, as well as side scatter height versus width for a total of three dual parameter plots to gate out aggregates and debris. We used single color controls to calculate compensation using the FACSDiva software. A plot of forward scatter versus PI fluorescence was used as the fourth gate to identify individual, live cells. To measure markers with the maximum sensitivity, each fluorochrome was plotted versus PI and polygons were drawn, angled with the aid of the Fluorescence Minus One controls. This excluded dead and autofluorescent cells, but included dim positives. By using polygon gates in combination with logical gates, inclusion of false-positive cells in the gates was reduced.

Macrophage migration assays

In vitro migration of macrophages was measured as described previously (Lee et al., 2011b). For preparation of ACM, primary adipocytes from HFD WT or HFD HAKO were incubated in Dulbecco's Modified Eagle's media supplemented with 0.2% BSA for 12 h. In vivo macrophage tracking experiments was performed as described previously (Oh et al., 2012). Leukocyte pools from C57BL/6 male 12-week-old mice, bled by retroorbital sinus, were

subjected to erythrocyte lysis, and monocyte subsets were enriched with the EasySep mouse monocyte enrichment kit (Stemcell Tech, Vancouver, BC, Canada), following the manufacturer's instructions. Isolated monocytes (5×10^6 to 10×10^6) were washed once in serum-free medium (RPMI-1640) and suspended in 2 mL diluent solution C (included in the PKH26 labeling kit). A total of 2 mL PKH26 (Sigma Chemical, St. Louis, MO) at 2×10^{-3} mol/L in diluent C was added and mixed, and the cells were incubated for 10 min at room temperature in the dark. The staining reaction was halted by the addition of an equal volume (2 mL) of medium supplemented with 10% FBS. The mixture was centrifuged, and the cells were washed once and resuspended in serum-containing medium. Subsequent to labeling with PKH26, the monocytes were counted and $\sim 1 \times 10^6$ viable cells were suspended in 0.2 mL PBS and injected into the femoral vein of the each group of mice. 7 days after the injection, the ATMs were immediately isolated from visceral fat tissue and analyzed by flow cytometry.

Measurement of protein nitrosylation

To measure protein S-nitrosylation, total lysates of epididymal adipose tissues from WT or HAKO mice fed normal chow or HFD were subjected to the biotin-switch assays (Cayman) according to the manufacturer's protocol. To assess total protein Snitrosylation, samples with the biotinylated nitrosocysteines were subjected SDS-PAGE electrophoresis, and immunoblottings with streptavidin conjugated with horseradish phosphatase. To assess Akt S-nitrosylation, samples with the biotinylated nitrosocysteines were immunoprecipitated with streptavidin-coated sepharose beads, and then subjected to immunoblottings with anti-Akt antidody.

Supplementary Material

Refer to Web version on PubMed Central for supplementary material.

Acknowledgments

This work was supported by the National Institutes of Health (NIH) grants DK-033651, DK-074868, DK-063491, and P01-DK054441. Y.S.L. was supported by a Mentor-Based Postdoctoral Fellowship Award from American Diabetes Association. S.S. is supported by the National Institute of Aging and National Institute of Child Health and Human Development of the National Institutes of Health (NIH) under award numbers, R01AG043120 and R24HD050837. R.S.J. is supported by a Principal Research Fellowship from the Wellcome Trust.

References

Ahmadian M, Abbott MJ, Tang T, Hudak CS, Kim Y, Bruss M, Hellerstein MK, Lee HY, Samuel VT, Shulman GI, et al. Desnutrin/ATGL is regulated by AMPK and is required for a brown adipose phenotype. Cell metabolism. 2011; 13:739–748. [PubMed: 21641555]

Andreyev A, Bondareva TO, Dedukhova VI, Mokhova EN, Skulachev VP, Volkov NI. Carboxyatractylate inhibits the uncoupling effect of free fatty acids. FEBS letters. 1988; 226:265–269. [PubMed: 3338558]

Barak Y, Liao D, He W, Ong ES, Nelson MC, Olefsky JM, Boland R, Evans RM. Effects of peroxisome proliferator-activated receptor delta on placentation, adiposity, and colorectal cancer. Proceedings of the National Academy of Sciences of the United States of America. 2002; 99:303–308. [PubMed: 11756685]

Branco-Price C, Zhang N, Schnelle M, Evans C, Katschinski DM, Liao D, Ellies L, Johnson RS. Endothelial cell HIF-1alpha and HIF-2alpha differentially regulate metastatic success. Cancer cell. 2012; 21:52–65. [PubMed: 22264788]

Chalkiadaki A, Guarente L. High-fat diet triggers inflammation-induced cleavage of SIRT1 in adipose tissue to promote metabolic dysfunction. Cell metabolism. 2012; 16:180–188. [PubMed: 22883230]

Deng T, Lyon CJ, Minze LJ, Lin J, Zou J, Liu JZ, Ren Y, Yin Z, Hamilton DJ, Reardon PR, et al. Class II major histocompatibility complex plays an essential role in obesity-induced adipose inflammation. Cell metabolism. 2013; 17:411–422. [PubMed: 23473035]

Doege K, Heine S, Jensen I, Jelkmann W, Metzen E. Inhibition of mitochondrial respiration elevates oxygen concentration but leaves regulation of hypoxia-inducible factor (HIF) intact. Blood. 2005; 106:2311–2317. [PubMed: 15947089]

Garcia-Arcos I, Hiyama Y, Drosatos K, Bharadwaj KG, Hu Y, Son NH, O'Byrne SM, Chang CL, Deckelbaum RJ, Takahashi M, et al. Adipose-specific lipoprotein lipase deficiency more profoundly affects brown than white fat biology. The Journal of biological chemistry. 2013; 288:14046–14058. [PubMed: 23542081]

Glass CK, Olefsky JM. Inflammation and lipid signaling in the etiology of insulin resistance. Cell metabolism. 2012; 15:635–645. [PubMed: 22560216]

Gonsalves CS, Kalra VK. Hypoxia-mediated expression of 5-lipoxygenase-activating protein involves HIF-1alpha and NF-kappaB and microRNAs 135a and 199a-5p. J Immunol. 2010; 184:3878–3888. [PubMed: 20194722]

Hagen T, Taylor CT, Lam F, Moncada S. Redistribution of intracellular oxygen in hypoxia by nitric oxide: effect on HIF1alpha. Science. 2003; 302:1975–1978. [PubMed: 14671307]

Halberg N, Khan T, Trujillo ME, Wernstedt-Asterholm I, Attie AD, Sherwani S, Wang ZV, Landskroner-Eiger S, Dineen S, Magalang UJ, et al. Hypoxia-inducible factor 1alpha induces fibrosis and insulin resistance in white adipose tissue. Molecular and cellular biology. 2009; 29:4467–4483. [PubMed: 19546236]

He W, Barak Y, Hevener A, Olson P, Liao D, Le J, Nelson M, Ong E, Olefsky JM, Evans RM. Adipose-specific peroxisome proliferator-activated receptor gamma knockout causes insulin resistance in fat and liver but not in muscle. Proceedings of the National Academy of Sciences of the United States of America. 2003; 100:15712–15717. [PubMed: 14660788]

Hosogai N, Fukuhara A, Oshima K, Miyata Y, Tanaka S, Segawa K, Furukawa S, Tochino Y, Komuro R, Matsuda M, et al. Adipose tissue hypoxia in obesity and its impact on adipocytokine dysregulation. Diabetes. 2007; 56:901–911. [PubMed: 17395738]

Jiang C, Qu A, Matsubara T, Chanturiya T, Jou W, Gavrilova O, Shah YM, Gonzalez FJ. Disruption of hypoxia-inducible factor 1 in adipocytes improves insulin sensitivity and decreases adiposity in high-fat diet-fed mice. Diabetes. 2011; 60:2484–2495. [PubMed: 21873554]

Keith B, Johnson RS, Simon MC. HIF1alpha and HIF2alpha: sibling rivalry in hypoxic tumour growth and progression. Nature reviews Cancer. 2012; 12:9–22.

Krishnan J, Danzer C, Simka T, Ukropec J, Walter KM, Kumpf S, Mirtschink P, Ukropcova B, Gasperikova D, Pedrazzini T, et al. Dietary obesity-associated Hif1alpha activation in adipocytes restricts fatty acid oxidation and energy expenditure via suppression of the Sirt2-NAD+ system. Genes & development. 2012; 26:259–270. [PubMed: 22302938]

Lee KY, Gesta S, Boucher J, Wang XL, Kahn CR. The differential role of Hif1beta/Arnt and the hypoxic response in adipose function, fibrosis, and inflammation. Cell metabolism. 2011a; 14:491–503. [PubMed: 21982709]

Lee YS, Choi JW, Hwang I, Lee JW, Lee JH, Kim AY, Huh JY, Koh YJ, Koh GY, Son HJ, et al. Adipocytokine orosomucoid integrates inflammatory and metabolic signals to preserve energy homeostasis by resolving immoderate inflammation. The Journal of biological chemistry. 2010; 285:22174–22185. [PubMed: 20442402]

Lee YS, Kim AY, Choi JW, Kim M, Yasue S, Son HJ, Masuzaki H, Park KS, Kim JB. Dysregulation of adipose glutathione peroxidase 3 in obesity contributes to local and systemic oxidative stress. Mol Endocrinol. 2008; 22:2176–2189. [PubMed: 18562625]

Lee YS, Li P, Huh JY, Hwang IJ, Lu M, Kim JI, Ham M, Talukdar S, Chen A, Lu WJ, et al. Inflammation is necessary for long-term but not short-term high-fat diet-induced insulin resistance. Diabetes. 2011b; 60:2474–2483. [PubMed: 21911747]

Lee YS, Morinaga H, Kim JJ, Lagakos W, Taylor S, Keshwani M, Perkins G, Dong H, Kayali AG, Sweet IR, et al. The fractalkine/CX3CR1 system regulates beta cell function and insulin secretion. Cell. 2013; 153:413–425. [PubMed: 23582329]

Leibel RL, Hirsch J, Berry EM, Gruen RK. Alterations in adipocyte free fatty acid re-esterification associated with obesity and weight reduction in man. The American journal of clinical nutrition. 1985; 42:198–206. [PubMed: 4025192]

Li P, Fan W, Xu J, Lu M, Yamamoto H, Auwerx J, Sears DD, Talukdar S, Oh D, Chen A, et al. Adipocyte NCoR knockout decreases PPARgamma phosphorylation and enhances PPARgamma activity and insulin sensitivity. Cell. 2011; 147:815–826. [PubMed: 22078880]

Melillo G, Taylor LS, Brooks A, Cox GW, Varesio L. Regulation of inducible nitric oxide synthase expression in IFN-gamma-treated murine macrophages cultured under hypoxic conditions. J Immunol. 1996; 157:2638–2644. [PubMed: 8805668]

Nielsen S, Guo Z, Johnson CM, Hensrud DD, Jensen MD. Splanchnic lipolysis in human obesity. The Journal of clinical investigation. 2004; 113:1582–1588. [PubMed: 15173884]

Oh DY, Morinaga H, Talukdar S, Bae EJ, Olefsky JM. Increased macrophage migration into adipose tissue in obese mice. Diabetes. 2012; 61:346–354. [PubMed: 22190646]

Pasarica M, Sereda OR, Redman LM, Albarado DC, Hymel DT, Roan LE, Rood JC, Burk DH, Smith SR. Reduced adipose tissue oxygenation in human obesity: evidence for rarefaction, macrophage chemotaxis, and inflammation without an angiogenic response. Diabetes. 2009; 58:718–725. [PubMed: 19074987]

Paschos GK, Ibrahim S, Song WL, Kunieda T, Grant G, Reyes TM, Bradfield CA, Vaughan CH, Eiden M, Masoodi M, et al. Obesity in mice with adipocyte-specific deletion of clock component Arntl. Nature medicine. 2012; 18:1768–1777.

Perreault M, Marette A. Targeted disruption of inducible nitric oxide synthase protects against obesity-linked insulin resistance in muscle. Nature medicine. 2001; 7:1138–1143.

Polak P, Cybulski N, Feige JN, Auwerx J, Ruegg MA, Hall MN. Adipose-specific knockout of raptor results in lean mice with enhanced mitochondrial respiration. Cell metabolism. 2008; 8:399–410. [PubMed: 19046571]

Rohm M, Sommerfeld A, Strzoda D, Jones A, Sijmonsma TP, Rudofsky G, Wolfrum C, Sticht C, Gretz N, Zeyda M, et al. Transcriptional cofactor TBLR1 controls lipid mobilization in white adipose tissue. Cell metabolism. 2013; 17:575–585. [PubMed: 23499424]

Sabio G, Das M, Mora A, Zhang Z, Jun JY, Ko HJ, Barrett T, Kim JK, Davis RJ. A stress signaling pathway in adipose tissue regulates hepatic insulin resistance. Science. 2008; 322:1539–1543. [PubMed: 19056984]

Sato Y, Endo H, Okuyama H, Takeda T, Iwahashi H, Imagawa A, Yamagata K, Shimomura I, Inoue M. Cellular hypoxia of pancreatic beta-cells due to high levels of oxygen consumption for insulin secretion in vitro. The Journal of biological chemistry. 2011; 286:12524–12532. [PubMed: 21296882]

Shu CJ, Benoist C, Mathis D. The immune system's involvement in obesity-driven type 2 diabetes. Seminars in immunology. 2012; 24:436–442. [PubMed: 23333525]

Sims K, Haynes CA, Kelly S, Allegood JC, Wang E, Momin A, Leipelt M, Reichart D, Glass CK, Sullards MC, et al. Kdo2-lipid A, a TLR4-specific agonist, induces de novo sphingolipid biosynthesis in RAW264.7 macrophages, which is essential for induction of autophagy. The Journal of biological chemistry. 2010; 285:38568–38579. [PubMed: 20876532]

Spite M, Hellmann J, Tang Y, Mathis SP, Kosuri M, Bhatnagar A, Jala VR, Haribabu B. Deficiency of the leukotriene B4 receptor, BLT-1, protects against systemic insulin resistance in diet-induced obesity. J Immunol. 2011; 187:1942–1949. [PubMed: 21742977]

Sridharan V, Guichard J, Li CY, Muise-Helmericks R, Beeson CC, Wright GL. O(2)-sensing signal cascade: clamping of O(2) respiration, reduced ATP utilization, and inducible fumarate respiration. American journal of physiology Cell physiology. 2008; 295:C29–37. [PubMed: 18463229]

Sun K, Halberg N, Khan M, Magalang UJ, Scherer PE. Selective inhibition of hypoxia-inducible factor 1alpha ameliorates adipose tissue dysfunction. Molecular and cellular biology. 2013; 33:904–917. [PubMed: 23249949]

Takeda N, O'Dea EL, Doedens A, Kim JW, Weidemann A, Stockmann C, Asagiri M, Simon MC, Hoffmann A, Johnson RS. Differential activation and antagonistic function of HIF-{alpha} isoforms in macrophages are essential for NO homeostasis. Genes & development. 2010; 24:491–501. [PubMed: 20194441]

Yasukawa T, Tokunaga E, Ota H, Sugita H, Martyn JA, Kaneki M. S-nitrosylation-dependent inactivation of Akt/protein kinase B in insulin resistance. The Journal of biological chemistry. 2005; 280:7511–7518. [PubMed: 15632167]

Zhang X, Lam KS, Ye H, Chung SK, Zhou M, Wang Y, Xu A. Adipose tissue-specific inhibition of hypoxia-inducible factor 1{alpha} induces obesity and glucose intolerance by impeding energy expenditure in mice. The Journal of biological chemistry. 2010; 285:32869–32877. [PubMed: 20716529]

Zhivotovsky B, Galluzzi L, Kepp O, Kroemer G. Adenine nucleotide translocase: a component of the phylogenetically conserved cell death machinery. Cell death and differentiation. 2009; 16:1419–1425. [PubMed: 19696789]

Highlights

- Saturated fatty acids activate adipocyte mitochondrial ANT2, elevating O_2 consumption.
- Increased O_2 consumption leads to relative adipocyte hypoxia and HIF-1α induction.
- HIF-1α promotes chemokine release from adipocytes, leading to adipose inflammation.
- Adipocyte HIF-1α KO protects from HFD-induced inflammation and insulin resistance.

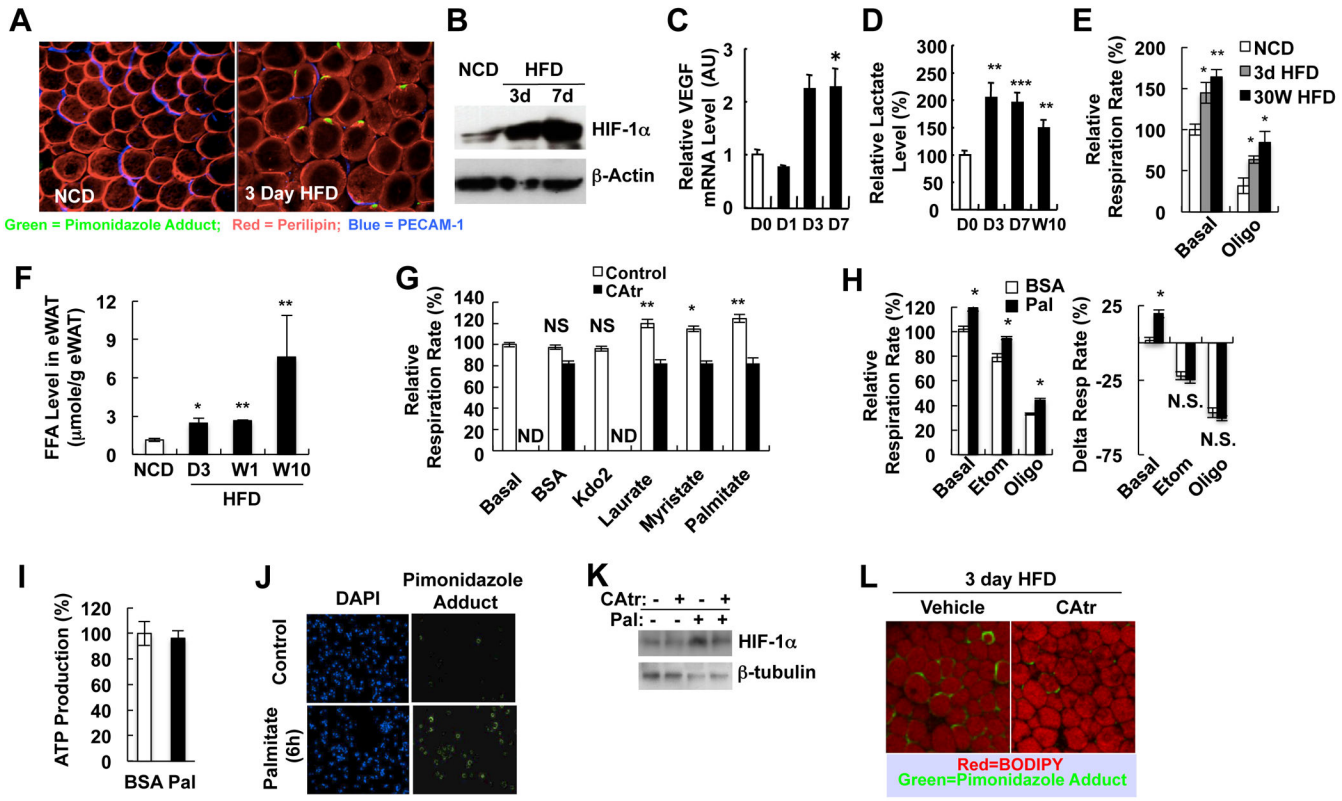

Figure 1.

Increased adipocyte oxygen consumption by FFA-induced uncoupled respiration contributes to adipose tissue hypoxia in obesity. (**A**) Whole-mount immunohistochemistry analysis of eWAT from mice fed normal chow diet (NCD) or HFD for 3 days. Green, pimonidazole adduct; Red, perilipin; Blue, PECAM-1. (**B**) Western blot analysis of HIF-1α in eWAT. (**C-D**) Q-PCR analysis of *VEGF* expression (**C**) or lactate concentration (**D**) in eWAT from mice fed NCD or HFD. D1, 1 day HFD; D3, 3 day HFD; D7, 7 day HFD; W10, 10 week HFD. n=8 per group. (**E**) Relative oxygen consumption rate in the presence or absence of oligomycin in primary adipocytes from NCD/lean or HFD/obese mice. n=4 per group. (**F**) FFA level in eWAT of NCD or HFD mice. n=5-7 per group. *, P<0.05; **, P<0.01. (**G**) Oxygen consumption rate in 3T3-L1 adipocytes before and after BSA, KLA (Kdo2), or each of FFAs indicated (50 μM) in the presence or absence of an inhibitor of ANT, carboxyatractyloside (CAtr). *, P<0.05; **, P<0.01. (**H**) Palmitate-induced respiration is not inhibited by Etomoxir (Etom) or oligomycin (Oligo). (**I**) ATP production as calculated from Seahorse data as described previously (Sridharan et al., 2008). (**J**) Palmitate induces hypoxia (pimonidazole adducts) in cultured 3T3-L1 adipocytes. Detailed protocols are described in the Extended Experimental Procedures. Blue, DAPI; Green, hypoxia probe. (**K**) Western blot analysis of HIF-1α protein in 3T3-L1 adipocytes with or without palmitate (100 μM) and/or CAtr (1 μM). (**L**) Acute injection of CAtr reduces adipocyte hypoxia in mice fed a HFD for 3 days. Green, hypoxia probe; Red, BODIPY. All data are mean+/-SEM. See also Figure S1.

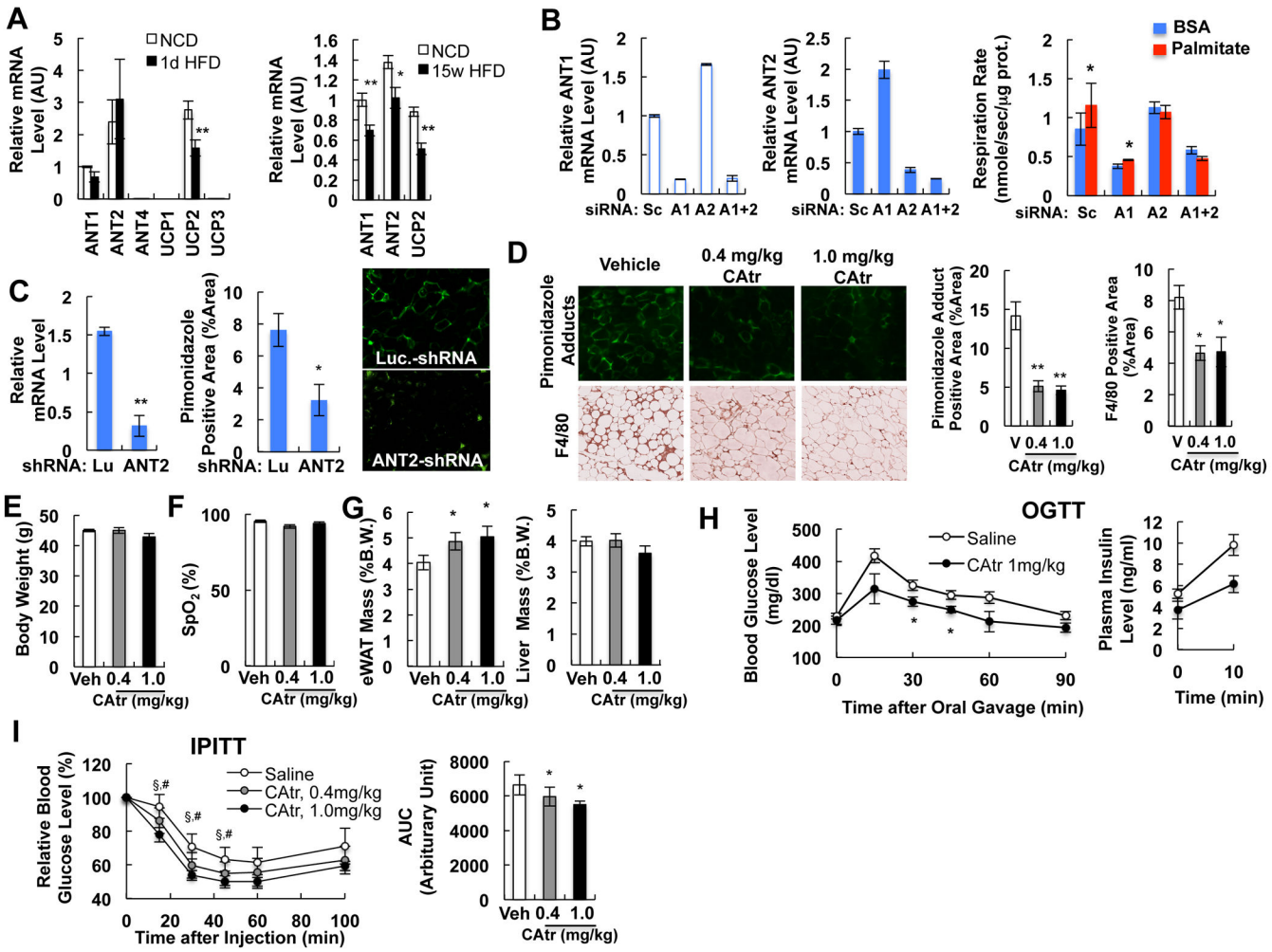

Figure 2.

Effects of ANT inhibition in obesity. (**A**) Expression of different isoforms of *ANT* and *UCP* genes in isolated primary eWAT adipocytes of chow or HFD mice at 1 day (left) or 15 weeks (right). *, P<0.05; **, P<0.01. (**B**) Effect of *ANT1* or *ANT2* knock down in 3T3-L1 adipocytes. 3T3-L1 adipocytes were transfected with scrambled siRNA (Sc) or siRNAs against *ANT1*(A1) *or ANT2* (A2), or both (A1+2), and oxygen consumption rate was measured using Clark type electrode. *, P<0.05. (**C**) In vivo *ANT2* knockdown decreases adipose tissue hypoxia. Green staining (middle panel) represents pimonidazole adduct-positive area. *, P<0.05; **, P<0.01. (**D-I**) Effect of chronic CAtr treatment on hypoxia (**D**), body weight (**E**), blood oxygenation (**F**), eWAT and liver weight (**G**), glucose tolerance (**H**) and insulin tolerance (**I**) at day 5-9. The graph shows body weight at day 5. *, P<0.05; **, P<0.01; § , P<0.05 0.4 mg/kg CAtr vs control; ; #, P<0.05 1.0 mg/kg CAtr vs control. See also Figure S2.

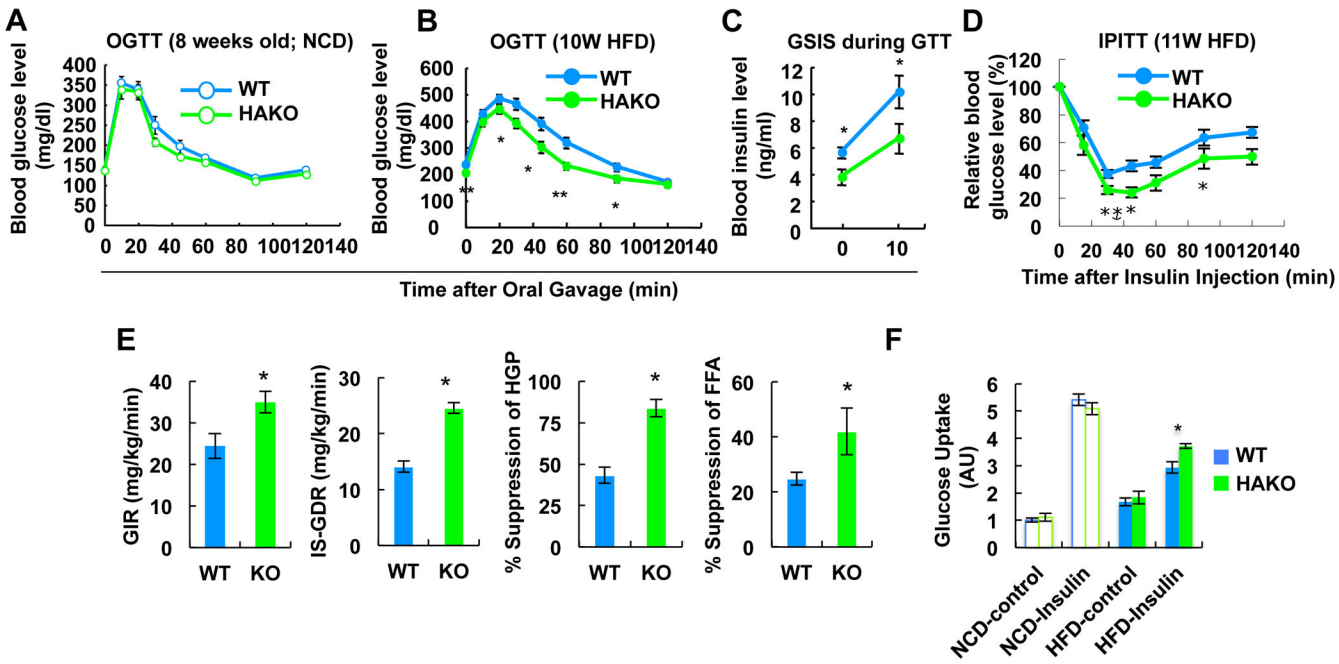

Figure 3.

HIF-1α KO mice exhibit improved glucose tolerance and insulin sensitivity on HFD. (**A**) GTT with mice fed NCD. (**B**) GTT with mice fed HFD for 10 weeks. (**C**) Plasma insulin level during GTT in panel B. (**D**) ITT in mice fed HFD for 11 weeks. (**E**) Hyperinsulinemic euglycemic clamp performed on mice fed a HFD for 15 weeks. (**F**) Glucose uptake assays using primary adipocytes from WT or HAKO mice fed HFD for 15 weeks. All data represent mean+/-SEM. See also Figure S3.

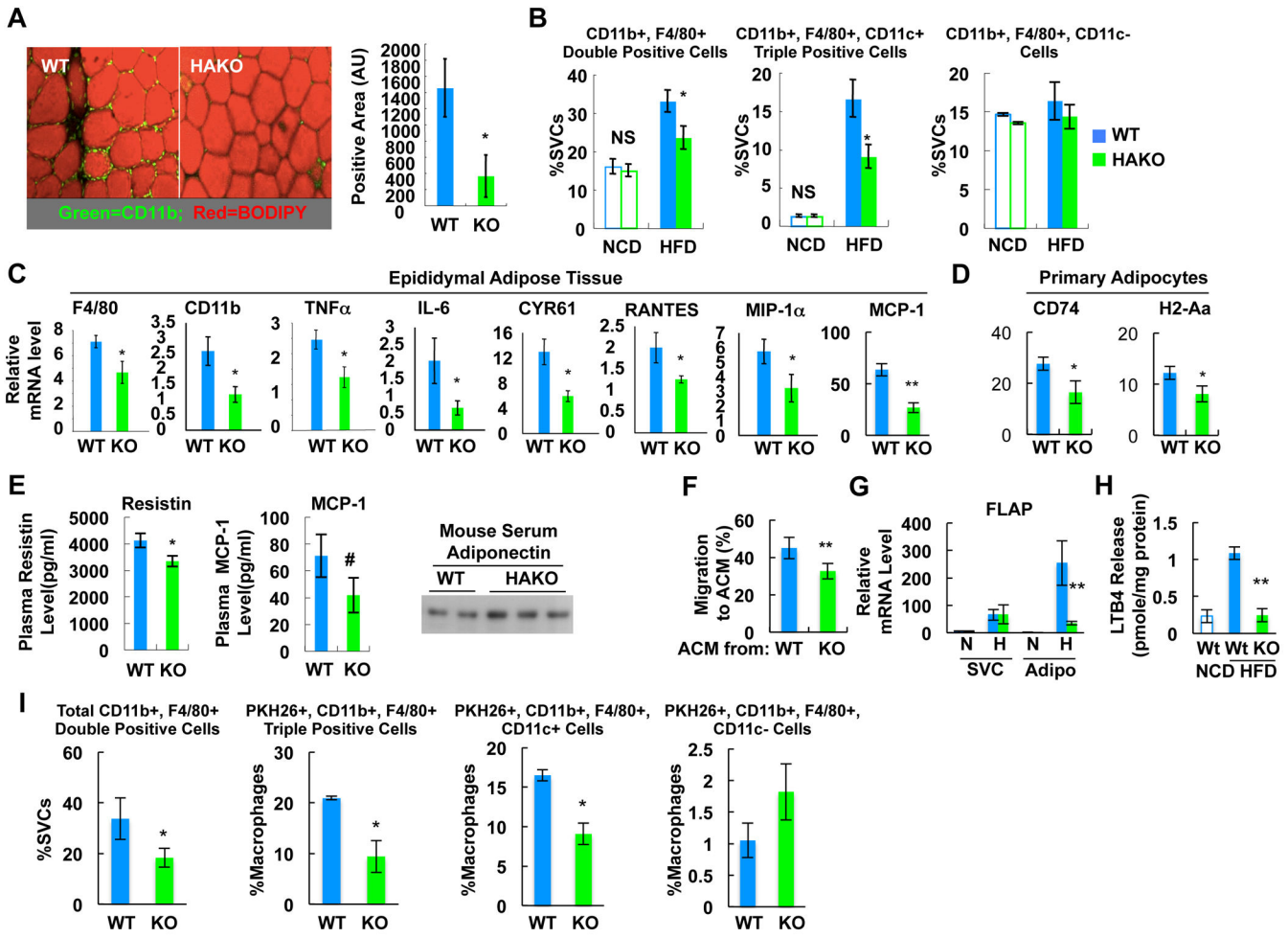

Figure 4.

HAKO mice exhibit reduced macrophage infiltration and inflammatory gene expression with reduced chemokine and LTB4 production. (**A**) IHC analysis of ATMs from WT or HAKO mice fed a HFD for 15 weeks. Red, neutral lipids (BODIPY); green, macrophage (CD11b). n=5 or 6 per group. (**B**) Flow cytometry analysis of eWAT SVCs from 15 week HFD mice. n=4 (NCD) or 7 (HFD) per group. (**C**) mRNA levels of inflammatory genes in adipose tissue were measured by RT-PCR analysis. n=6. (**D**) mRNA levels of class II MHC genes in primary adipocytes were measured by RT-PCR. n=7 per group. (**E**) Plasma levels of adipokines (n=7) as measured by ELISA or western blots. (**F**) Chemoattractive activity of ACM harvested from HAKO adipocytes is reduced compared with WT adipocytes (15 week HFD). n=4 per group. (**G**) *FLAP* mRNA level in adipocyte and SVC fractions of eWAT from mice fed NCD or HFD (15 weeks). n=7 or 9 per group. (**H**) LTB4 release from isolated adipocytes of NCD WT, HFD WT or HFD HAKO mice. n=3 or 7 per group. (**I**) In vivo monocyte tracking (n=4). All data represent mean+/-SEM. See also Figure S4.

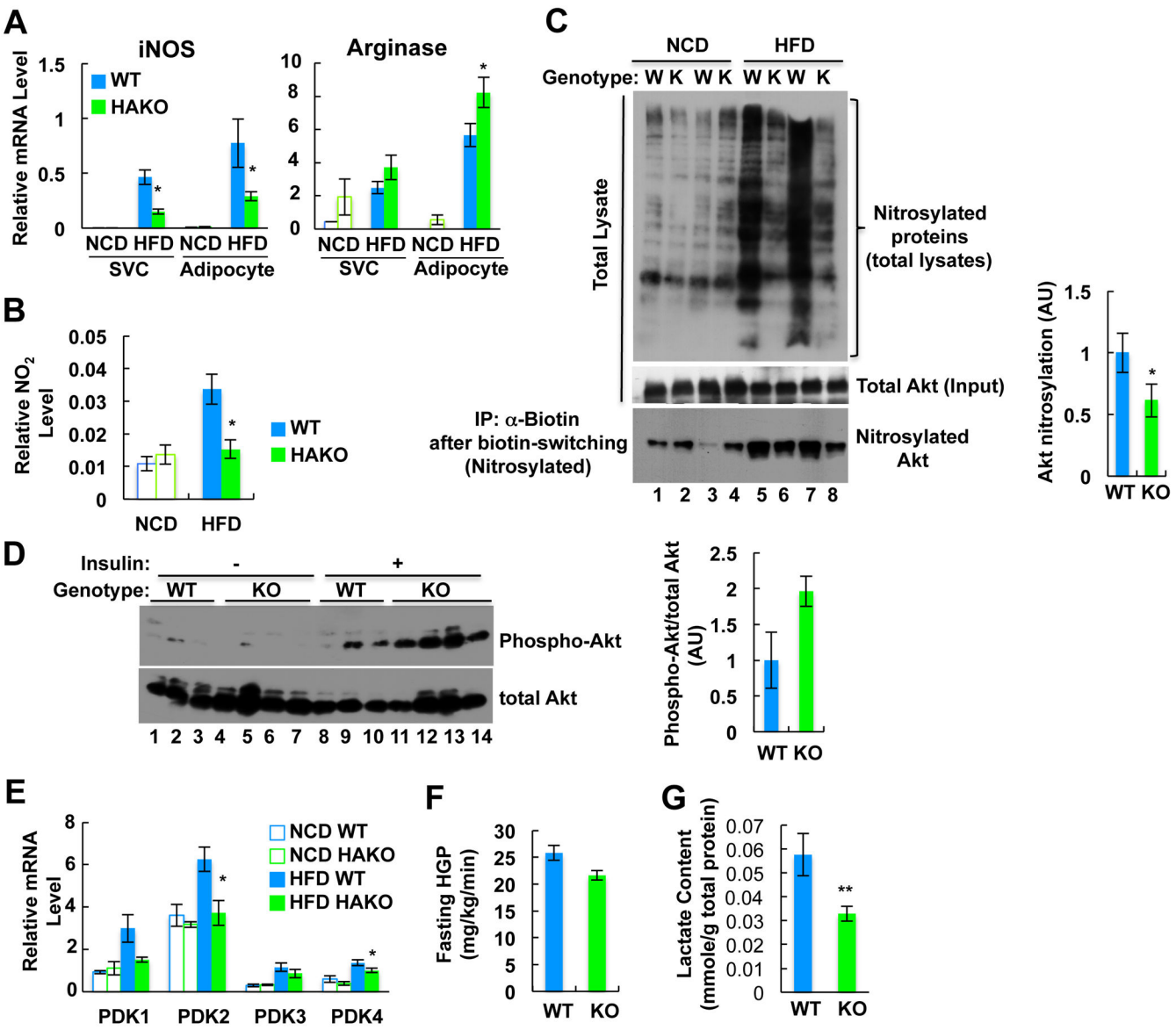

Figure 5.

HAKO mice fed a HFD show reduced NO production and Akt nitrosylation, and lower lactate production in adipocytes. (**A**) mRNA levels of *iNOS* and *arginase 1* in adipocyte and eWAT SVCs from WT and HAKO mice. n=4 or 7 per group. (**B**) Nitrite level in eWAT of WT and HAKO mice. n=4 or 5 per group. (**C**) HFD-induced nitrosylation of Akt and total protein in adipose tissue is reduced by HAKO. (**D**) Akt phosphorylation in eWAT from WT or HAKO mice before and after insulin injection. (**E**) PDK expression. n=4 or 7 per group. (**F**) Fasting hepatic glucose production (HGP) is lower in HAKO mice on HFD. (**G**) Adipose tissue lactate content is decreased in HAKO mice. n=5 per group. All data represent mean+/-SEM.

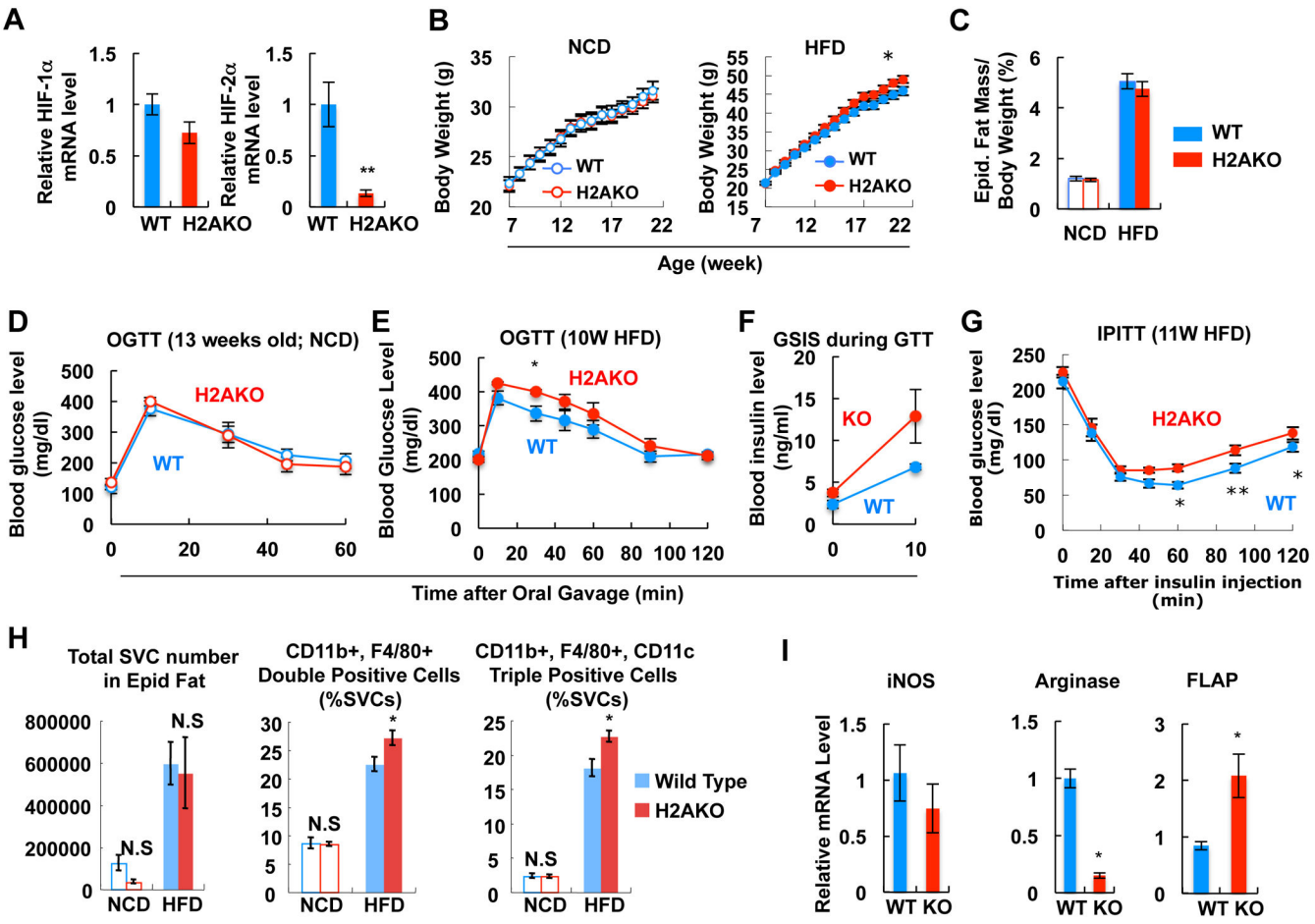

Figure 6.

H2AKO impairs glucose and insulin tolerance with increased adipose tissue inflammation. (**A**) mRNA levels *of HIF-1α* and *HIF-2α* in adipose tissue of HFD WT or H2AKO mice. n=6. (**B**) Body weight of WT and H2AKO mice fed NCD (n=10) or HFD (n=36). (**C**) eWAT mass on NCD and HFD (15 weeks; n=5 per group). (**D**) GTT in NCD mice. (**E**) GTT performed in 10 week HFD mice. (**F**) Plasma insulin level during GTT in panel **E**. (**G**) ITT test with mice on 11 week HFD. (**H**) Flow cytometry analysis of eWAT SVCs. n=4 or 9 per group. (**I**) RT-PCR analysis of inflammatory gene expression in primary adipocytes from HFD WT or HFD H2AKO mice. n=6 per group. All data represent mean+/-SEM. See also Figure S5.

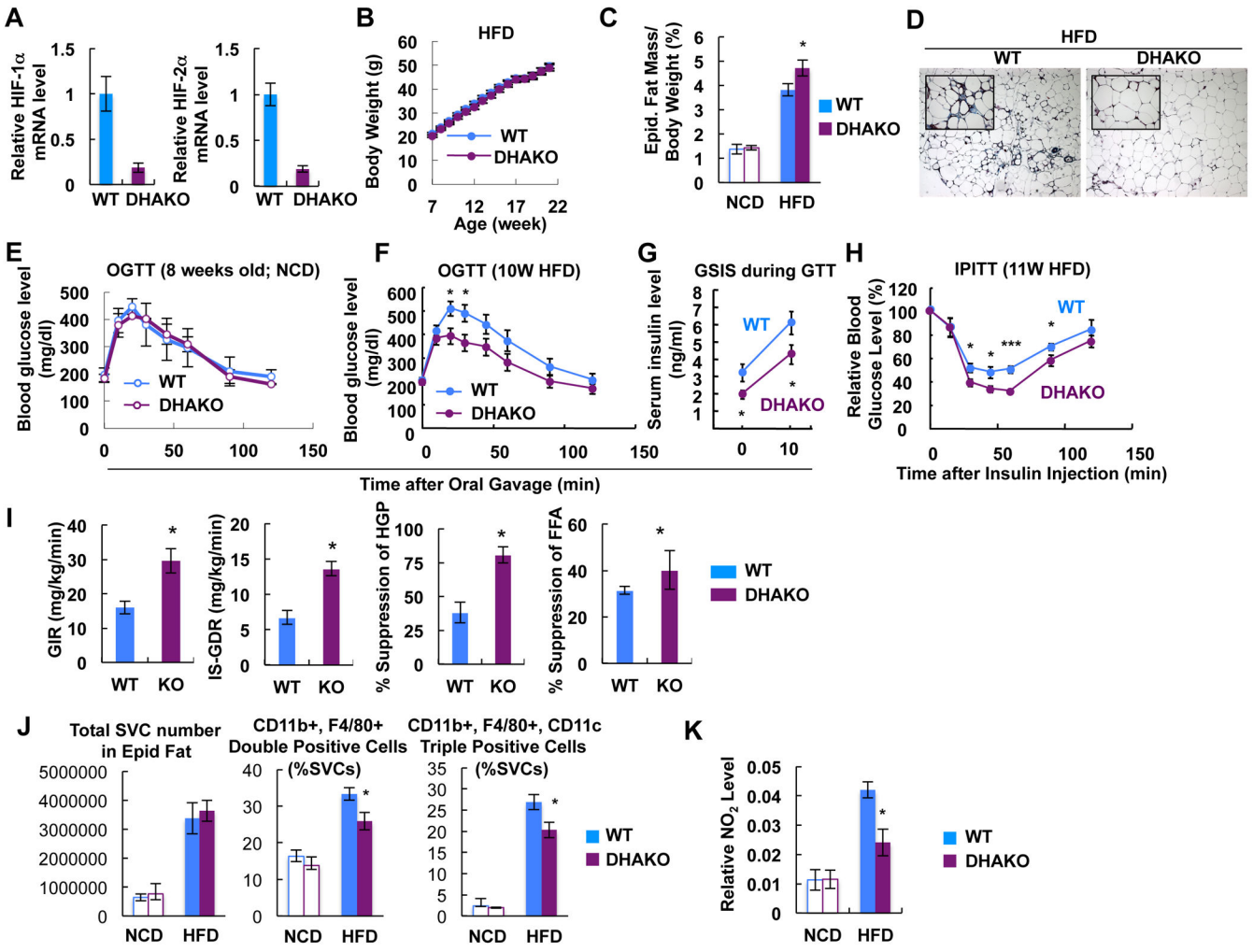

Figure 7.

DHAKO mice exhibit similar metabolic changes to HAKO mice. (**A**) mRNA levels of *HIF-1α* and *HIF-2α* in adipose tissue of HFD WT or DHAKO mice. (**B**) B.W. of WT and DHAKO mice on HFD. n=18 or 20 per group. (**C**) eWAT mass on NCD and HFD (15 weeks). n=7 or 10 per group. *, P<0.05. (**D**) Trichrome (blue) and H&E stainings of eWAT from mice fed a HFD for 15 weeks. (**E-F**) GTT in mice fed a NCD (**E**) or HFD for 10 weeks (**F**). *, P<0.05. (**G**) Plasma insulin level during GTT in panel **F**. (**H**) ITT in mice fed a HFD for 11 weeks. *, P<0.05; ***, P<0.001. (**I**) Hyperinsulinemic euglycemic clamp with mice fed a HFD for 15 weeks. *, P<0.05. (**J**) Flow cytometry analysis of eWAT SVCs. n=7 or 10 per group. *, P<0.05. (**K**) Nitrite level in eWAT of WT and DHAKO mice on chow or HFD. n=4 or 5 per group. *, P<0.05. All data represent mean+/-SEM.